Structure–Functional Relationships of Ni/Zeolite Composites in CO_2 Reforming of Methane

Jafarova Sevil Tagi
Ministry of Science and Education of Azerbaijan,
Institute of Chemistry Public Legal Entity, Baku - 1143, Azerbaijan
rsevil7@gmail.com

(Received on 30th March 2026, accepted in revised form 2nd July 2026)

Summary: This study investigates the comparative structure–function relationships of Ni/zeolite composites, Ni–X (X = CaA, NaX, CaX, NaY, ZSM-5, MOR, and clinoptilolite (CL)), for syngas production via dry reforming of methane (DRM). Particular attention is paid to the influence of zeolite framework topology, cationic composition, textural characteristics, and surface acid–base properties on catalytic performance under identical experimental conditions.

Characterization of a representative sample by XRD and SEM/EDX demonstrated the successful incorporation of nickel into the composite while maintaining the zeolite framework. In contrast to studies focused on individual zeolite systems, this work presents a comparative evaluation of Ni/zeolite catalyst representing a wide range of framework types, thus providing a robust basis for identifying structure–function relationships and their quantitative trends. The quantitative correlations identified between zeolite structure and the principal catalytic performance parameters for Ni/zeolites systems based on A-, X-, and Y-type, together with the higher activity of the narrow-pore Ni–CaA and Ni–CL catalysts, demonstrate the important role of framework topology in determining catalytic performance. Furthermore, analysis of the relationship between catalytic performance and surface acid–base properties highlighted the contribution of Lewis acidic and basic sites.

The work examines both structure–function relationships across different zeolite topologies and catalytic changes induced within the same framework type by physicochemical modification. Clinoptilolite-based catalysts demonstrated promising performance: acid activation of clinoptilolite enabled controlled tuning of the SiO_2/Al_2O_3 ratio, porosity, and surface acidity, leading to enhanced catalytic behavior. Overall, the catalytic performance of Ni-zeolite systems in DRM is governed by the interaction between framework structure, pore accessibility, cationic composition, and surface acid-base properties.

Keywords: Structure–function relationships, Ni/zeolite catalysts, Acid–base properties, Dry reforming of methane, Natural zeolites, Clinoptilolite.

Introduction

Synthesis gas (syngas) is an important feedstock for the production of a wide range of valuable chemicals and is also considered a promising energy carrier, particularly for environmentally friendly energy systems, including fuel cells [1, 2]. Natural gas remains the main source for syngas production due to the availability of well-established processing technologies. For gas streams containing significant amounts of CO_2, including biogas composed mainly of CH_4 and CO_2, dry reforming of methane (DRM) represents a promising route for syngas generation [2–4].

Dry reforming of methane ($CH_4 + CO_2 \rightarrow 2CO + 2H_2$) is attractive because it enables the simultaneous utilization of two greenhouse gases and converts CO_2-containing streams into valuable products [5–9].

Nickel-based catalysts are widely used in DRM due to their high activity in C–H bond activation and relatively low cost compared to noble metals [10, 11]. However, their practical application is limited by catalyst deactivation caused mainly by carbon deposition and sintering of the active phase [12-14]. These effects strongly depend on the nature of the support, nickel dispersion, and its surface properties [15-18].

The use of composite catalysts based on modified supports is an effective approach to improving catalytic stability and performance [19–22]. In particular, supports with basic properties or those modified with alkali and alkaline-earth metals can enhance nickel dispersion, improve CO_2 adsorption, and suppress carbon formation [23–25]. Such approaches are widely used in catalytic systems to increase resistance to deactivation [26–35].

Among various supports, zeolites have attracted considerable attention due to their well-defined framework structure, tunable SiO_2/Al_2O_3 ratio, pore architecture, and adjustable acid–base properties [36–41]. Their three-dimensional framework forms a system of interconnected cavities accessible through well-defined pore openings, near which charge-compensating exchangeable cations (e.g., Na^+,

*To whom all correspondence should be addressed.

Ca^{2+}, and K^{+}) are located. Variations in the crystal framework and in the nature of the exchangeable cations largely determine adsorption and catalytic behavior [41–43]. In addition, the zeolite framework can promote high dispersion of metal particles by spatially isolating the active species and inhibiting their aggregation [43–46].

Recent studies have shown that the physicochemical properties of zeolites-supports strongly influence metal dispersion, metal–support interaction, and catalytic performance in a range of CH_4 and CO_2 conversion reactions [47–49]. However, despite numerous studies on Ni-based catalysts, a comprehensive understanding of how zeolite framework topology and surface acid–base properties jointly affect catalytic performance in DRM remains limited [50].

The framework characteristics of zeolites are strongly influenced by the aluminum content and the corresponding SiO_2/Al_2O_3 ratio, which significantly affect the acid–base properties and catalytic behavior [51-53]. Brønsted acid sites are generally associated with framework Si–OH–Al groups, whereas Lewis acid sites are related to extra-framework aluminum species. Basic sites, in turn, are important for CO_2 adsorption and activation. Nevertheless, the role of different acid–base sites in methane activation and overall DRM performance remains under discussion [37, 54–57].

Thus, the relationship between zeolite structure, acid–base properties, and catalytic activity in DRM remains insufficiently understood. Unlike most previous studies, which often focus on individual catalyst systems, this work attempts to establish comparative and quantitative structure–function relationships for Ni/zeolite composites. Such an approach may contribute to the rational design of efficient catalysts for DRM.

Therefore, the aim of the present work was to investigate comparative structure–function relationships in Ni–X systems (X = CaA, CaX, NaX, NaY, ZSM-5, MOR, and clinoptilolite) and to evaluate the influence of zeolite framework structure, composition, textural characteristics, and surface acid–base properties on catalytic performance in the dry reforming of methane.

Experimental

A series of Ni–X composites was prepared using granulated commercial synthetic zeolites with well-defined framework topologies (A, X, and Y) as reference matrices to enable a comparative evaluation of structure–function relationships under identical DRM conditions. Mordenite (MOR) and ZSM-5, synthetic chabazite (Ch) were additionally included to assess the influence of framework structure and compositional variations, whereas clinoptilolite (CL) was used to examine such variations within a single framework type.

Thus, two series of Ni–X catalysts were investigated. The first included zeolites with different framework structures, pore topologies, and compositions (X = CaA, NaX, CaX, NaY, ZSM-5, and MOR), whereas the second comprised clinoptilolite-based catalysts used to examine structural and textural variations within the same zeolite framework type.

Natural clinoptilolite (SiO_2/Al_2O_3 = 8.68) and mordenite (SiO_2/Al_2O_3 = 9.6; mineral content 70–75 wt.%) from the Aidag and Chananab deposits (Azerbaijan), respectively, were used as catalyst supports. The natural clinoptilolite consisted of 78 ± 2 wt.% clinoptilolite, 15 ± 1 wt.% quartz, and 2 ± 0.5 wt.% calcite.

The Ni–X catalysts were prepared by incipient wetness impregnation method using an aqueous solution of nickel (II) nitrate hexahydrate, $Ni(NO_3)_2 \cdot 6H_2O$ (0.58 M, 17.4 g per 100 g support for nominal 10 wt.% NiO). The impregnated samples were dried at 110 ^{0}C for 4 h and calcined in air at 500 °C for 6 h. Prior to catalytic testing, the samples were reduced in a hydrogen flow (45 mL min^{-1}) at 400 °C for 5 h.

For the second series of experiments, Ni-CL catalysts with a modified support were prepared. To obtain the modified support, natural clinoptilolite (2 mm fraction) was treated with an HCl solution (0.5, 1, 2, and 10 M) at 60°C for 3 h (solid-to-liquid ratio 1:10). The treated samples were washed with distilled water until chloride-free ($AgNO_3$ test), dried at 110°C, and calcined at 400°C for 2 h. The obtained samples were designated CL-0.5, CL-1, CL-2, and CL-10, respectively. The physicochemical parameters of the acid-modified supports were determined and, for clarity, are summarized in Table 4. The subsequent procedure for the preparation of Ni catalysts based on these modified supports was analogous to that used for the Ni–X catalysts described above.

A detailed structural characterization (XRD, SEM/EDX) of the Ni–CL sample was performed. This sample was selected because clinoptilolite-based catalysts served as a model system for studying the effect of physicochemical changes on activity within the same framework type. Unlike the commercial reference zeolites used in this study, clinoptilolite exhibits less uniform structural and compositional characteristics. Therefore, detailed characterization was necessary to verify preservation of the zeolite framework after Ni incorporation.

X-ray diffraction (XRD) analysis was performed on a D2 Phaser diffractometer (Bruker, Germany) using $Cu_{K\alpha}$ radiation (λ = 1.54 Å) with a nickel filter in the 2θ range of 5–80°.

Surface morphology was investigated by scanning electron microscopy (SEM) on a Sigma VP microscope (Carl Zeiss, Germany) at 15 kV and ~20,000× magnification, coupled with energy-dispersive X-ray spectroscopy (EDX) for elemental composition.

Acid–base properties were examined using molecular probes (acetone as an electron-acceptor probe, n-butylamine as a proton-donor probe, phenol as a basic probe) via adsorption followed by «Paulik-Paulik-Erdei» derivatography [59]. Total acidity was expressed as ΣK_{NH3} (mmol g^{-1}) and determined from NH_3 desorption. This approach was used to estimate the concentration and nature of active surface sites and to evaluate their correlation with catalytic performance in DRM.

Catalytic performance was evaluated in a laboratory-scale continuous-flow quartz fixed-bed reactor at atmospheric pressure (1 atm). The reaction temperature (500–800°C) was measured by a chromel–alumel thermocouple at the catalyst bed center. Catalytic activity for all catalyst systems was evaluated under identical DRM conditions to ensure reliable comparative evaluation. Catalytic tests were carried out using a CH_4–CO_2 mixture (CH_4: CO_2 =1:1, GHSV 500 h^{-1}); products were analyzed by LCHM-80 gas chromatograph [60]. Conversions (X, %) and selectivity (S, %) were calculated as

$$X(CH4, CO2) = \frac{Fi - Ff}{Fi} \times 100\%$$

$$S(H2) = \frac{F(H2)f}{2 \times (F(CH4)i - F(CH4)f} \times 100\%$$

$$S(CO) = \frac{F(CO)f}{(F(CH4)i - F(CH4)f) + (F(CO2)i - F(CO2)f)} \times 100\%$$

where F_i and F_f are initial/final concentrations. Experiments were performed in duplicate to ensure reproducibility. CH_4 conversion, residual CO_2, H_2 yield, and H_2 selectivity were used as the main parameters for evaluating catalytic performance. Since this work is a comparative study of selected catalyst systems under fixed DRM conditions (500–800 °C, CH_4:CO_2 = 1:1, GHSV 500 h^{-1}), the conclusions are focused primarily on the observed structure – activity relationships, while correlation coefficients (r) were used to quantify the observed trends.

Results and discussion

To elucidate structure–activity relationships, a comparative analysis of the catalytic behavior of Ni–X systems with different zeolite framework types (X = NaY, NaX, CaX, CaA) was initially performed under identical conditions for DRM. The results of the study are presented in Fig. 1.

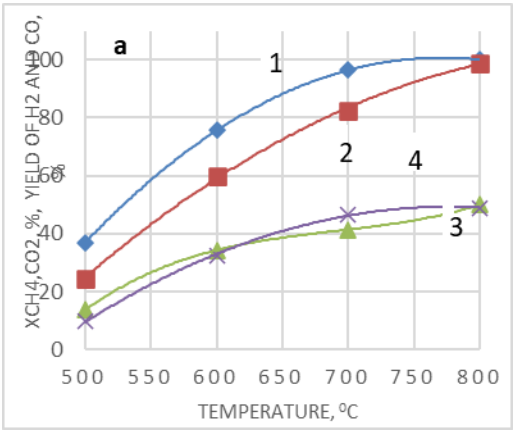

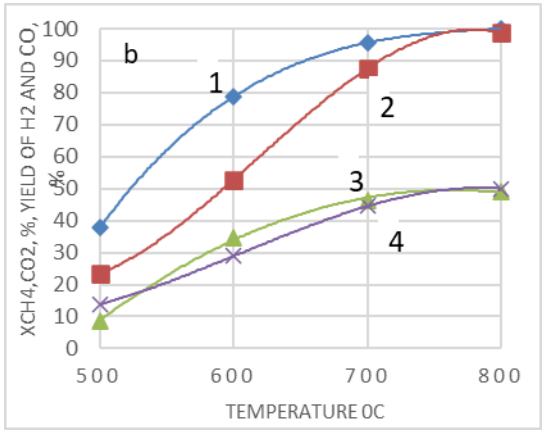

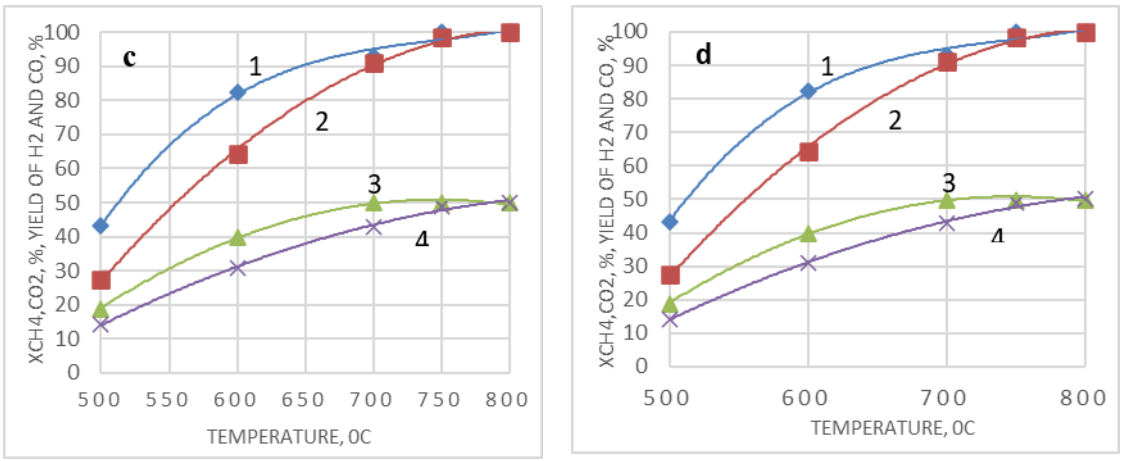

Fig. 1: Temperature dependences of CH_4 and CO_2 conversion and H_2 and CO yields in DRM over: (a) Ni–NaY, (b) Ni–NaX, (c) Ni–CaX, (d) Ni–CaA catalysts. Curves: (1) CH_4 conversion, (2) CO_2 conversion, (3) H_2 yield, (4) CO yield.

Table-1: Relationship between zeolite framework type and the catalytic performance of Ni–X (X = NaY, NaX, CaX, CaA) systems in DRM. *Selected parameters at 700 °C, vol.%.*

№	Zeolite	SiO_2/Al_2O_3 ratio, (mol/mol)	$T_{80\%}$ CH_4, ^0C	CH_4 conversion (X_{CH4})	H_2 yield	Residual CO_2 concentration
1	CaA	1.9	590	93.0	49.9	4.4
2	NaX	2.75	622	95.6	45.0	7.8
3	CaX	2.9	605	95.6	46.3	6.2
4	NaY	5.6	615	96.4	41.4	8.7
Correlation			0.52	0.765	-0.92	0.815

For all catalysts, CH_4 and CO_2 conversions, as well as H_2 and CO yields, increased with temperature, reflecting the thermally activated nature of the process. Complete methane conversion was achieved at 800 °C for Ni–NaY, Ni–NaX, and Ni–CaX, whereas the Ni–CaA catalyst reached full conversion at a lower temperature of 750 °C, evidencing its higher catalytic activity.

Additional experiments showed that the corresponding nickel-free samples (NaY, NaX, and CaX) exhibited no measurable catalytic activity under DRM conditions, highlighting the essential role of nickel sites in methane activation. In contrast, the nickel-free CaA zeolite, which likely possesses a higher CO_2 adsorption capacity, showed some activity, with CH_4 and CO_2 conversions of 11.46 ± 0.74 vol% and 10.53 ± 2.06 vol%, respectively. This was accompanied by relatively low H_2 and CO yields, both reaching 5.5 ± 0.7 vol%. Taken together, these results suggest that increased CO_2 uptake contributes to improved CH_4 conversion on Ni–CaA. Consequently, the observed differences between the Ni-X catalysts are attributed to the influence of zeolite framework structure, exchangeable cation type on nickel site accessibility and surface acid–base properties.

Therefore, particular attention was paid to methane conversion, residual CO_2 concentration and hydrogen yield, since these parameters together reflect the efficiency of syngas formation. Quantitative relationships between catalytic parameters and zeolite structural characteristics are summarized in Table 1.

Under these conditions, methane conversion over Ni–X catalysts ranged from 93.0 to 96.4%, confirming their high activity below complete conversion temperatures. The Ni–CaA sample exhibited the highest H_2 yield, consistent with its enhanced performance observed in the temperature-dependent profiles. Catalysts containing Ca^{2+} cations demonstrated lower T_{80}% values than Na^+-containing analogues, indicating facilitated methane activation.

Residual CO_2 concentrations were consistently lower for Ca-based systems, supporting the role of Ca^{2+} ions in promoting CO_2 adsorption and its subsequent conversion. This observation is supported by the stronger correlation between zeolite structure and residual CO_2 concentration (r = 0.815) than with methane conversion (r = 0.765).

The correlation analysis presented in Table 2 (a, b) provides further insight into the role of zeolite framework type in governing both the surface chemistry and catalytic performance of Ni–X (X = NaX, CaX, CaA) catalysts in DRM.

Table-2: (a) Concentration of surface acid–base sites in Ni–X catalysts (X = NaX, CaX, CaA) and correlation with zeolite structure.

Nature of sites	Catalyst	Concentration of surface sites, mmol·g^{-1}	Correlation coefficient (r)
Electron-acceptor acidic sites	**Ni-NaX**	**0.370**	**-0.999**
	Ni-CaX	**0.123**	
	Ni-CaA	**1.539**	
Proton-donor acidic sites	**Ni-NaX**	**0.734**	**-0.974**
	Ni-CaX	**0.098**	
	Ni-CaA	**1.859**	
Basic sites	**Ni-NaX**	**0.207**	**-0.999**
	Ni-CaX	**0.041**	
	Ni-CaA	**1.370**	

Note: Electron-acceptor, proton-donor acidic and basic sites were determined by the molecular probe adsorption method [57]. Correlation coefficients were calculated to evaluate the relationship between the zeolite framework and the concentration of surface acid–base sites.

Table -2(b): Correlation between surface acid–base site concentration and catalytic performance parameters of Ni–X catalysts in DRM.

Nature of sites	H_2 yield	S_{H2}	T_{80}% of CH_4 conversion	Residual CO_2 concentration
Electron-acceptor acidic sites	**0.91**	**0.935**	**-0.75**	**-0.79**
Proton-donor acidic sites	**0.81**	**0.85**	**-0.60**	**-0.65**
Basic sites	**0.93**	**0.95**	**-0.78**	**-0.82**

Note: Correlation coefficients (r) were calculated to evaluate the relationship between the concentration of surface acid–base sites and the catalytic performance parameters. Catalytic performance parameters were obtained from DRM catalytic tests.

A strong correlation between the zeolite structure and the concentration of surface acid–base sites confirms that the acid–base properties are primarily dictated by the framework composition and topology (Table 2 (a)).

In agreement with the trends discussed above, an increase in the SiO_2/Al_2O_3 ratio leads to a decrease in the concentration of both acidic and basic sites, due to the reduced fraction of aluminosilicate units responsible for active site formation. In the present study, the proton-donor acidic sites determined by molecular probe adsorption can be associated predominantly with Bronsted acidity of the aluminosilicate framework, whereas the electron-acceptor acidic sites correspond mainly to Lewis acidic centers related to coordinately unsaturated cations and defect sites.

The CaA-based catalyst, characterized by the smallest pore aperture, exhibits the highest density of surface sites, which likely promotes stronger confinement effects and a greater density of accessible acid–base centers (Table 2(a)). This behavior is consistent with its superior catalytic performance observed in Fig. 1 and Table 1. In particular, basic and Lewis-type acidic sites show the strongest correlation with catalytic performance parameters (Table 2(b)). Strong positive correlations with H_2 yield and selectivity ($S_{(H_2)}$), together with negative correlations with $T_{80\%}$, indicate that an increased density of these sites promotes methane activation and enhances overall reaction efficiency. Furthermore, the negative correlation between the concentration of basic sites and residual CO_2 concentration confirms their key role in CO_2 adsorption and activation.

Overall, the combined analysis of Tables 1 and 2 and Fig. 1 demonstrates that the catalytic performance of Ni–X systems is governed by an inter play between zeolite structure, pore geometry, and surface acid–base properties.

To further expand the comparative analysis of structure–activity relationships in DRM, Ni–ZSM-5 (MFI-type) and Ni–MOR (MOR-type) catalysts were also investigated. These zeolites possess distinct framework topologies and channel architectures and are characterized by relatively high SiO_2/Al_2O_3 ratios compared with the previously investigated zeolites, allowing further evaluation of how these structural features may influence reactant accessibility and catalytic behavior. According to literature data [61], ZSM-5 possesses channel openings of approximately 0.54–0.56 nm, whereas MOR is characterized by larger 12-membered-ring channels (about 0.65–0.70 nm), which can facilitate diffusion and improve accessibility of reactants and products; in addition, the 8-membered side channels of MOR are less accessible and may be partially blocked by cations or impurities. In contrast, ZSM-5 exhibits a more pronounced molecular-sieve effect. The results are presented in Fig. 2.

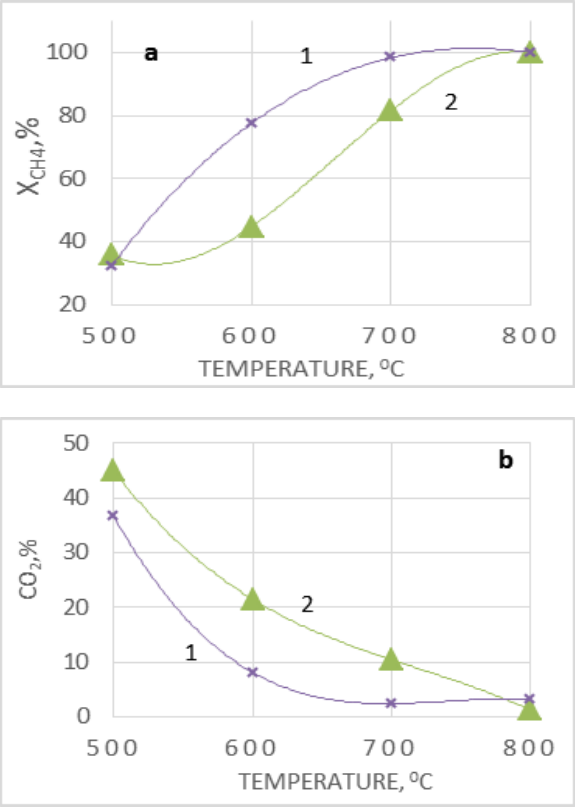

Fig. 2: Comparative temperature dependence of (a) CH_4 conversion and (b) residual CO_2 concentration over Ni–ZSM-5 and Ni–MOR catalysts in DRM. Curves: (1) Ni–ZSM-5 and (2) Ni–MOR.

As shown in Fig. 2, CH_4 conversion over Ni–ZSM-5 reached 98.4% at 700 °C, whereas for Ni–MOR it was 81.6%. This difference can be attributed to the more effective contribution of acidic sites in the ZSM-5-based catalyst. At the same time, Ni–MOR exhibited lower residual CO_2 concentrations (1.2 vs. 3.1 vol.% at 800 °C), likely due to the presence of associated minerals containing alkaline-earth metal oxides (Ca and Mg), which enhance CO_2 adsorption via acid–base interactions and promote CO_2 activation.

The observed differences indicate that catalytic behavior is governed not only by the acidity of the zeolite matrix, but also by pore topology and accessibility of active sites. The higher CH_4 conversion over Ni–ZSM-5 is associated with a more favorable distribution of accessible active centers for methane activation, whereas the lower residual CO_2 over Ni–MOR reflects a stronger contribution of CO_2 adsorption and activation processes related to its mineral composition.

Further insight into the role of exchangeable cations was obtained using synthetic chabazite-based Ni–Ch catalysts as a controlled model system, allowing evaluation of the cationic effect within a comparable framework topology. This comparison was motivated by the results obtained for zeolite containing different exchangeable cations, which suggested that the nature of exchangeable cations may influence DRM behavior.

Fig 3 shows the temperature dependence of CH_4 conversion over Ni–Ch catalysts containing different exchangeable cations in DRM. The Na-form exhibits complete methane conversion, whereas the K-form reaches a maximum conversion of only about 85.8%, indicating a stronger contribution of the Na-form to the catalytic activity. This difference indicates a more favorable interaction between the zeolite matrix and Ni species in the Na-form catalyst, which is consistent with the lower onset temperature for H_2-reduction [58]. These results confirm that the nature of the zeolite cations has a significant impact on catalytic activity.

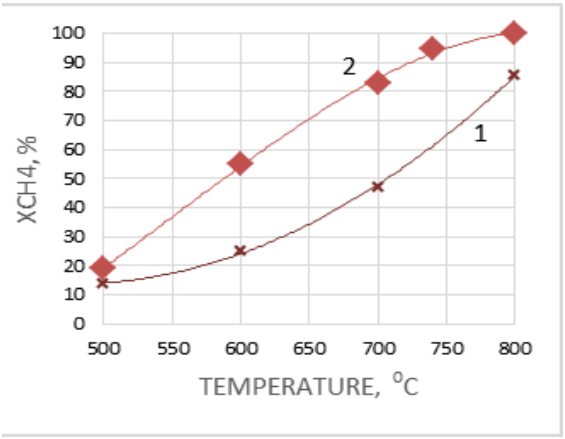

Fig. 3: Temperature dependence of CH_4 conversion over Ni–Ch catalysts containing different exchangeable zeolite cations in DRM. Curves: (1) K^+-form and (2) Na^+-form catalyst.

Table 3 summarizes the effect of the Na ion concentration on catalytic activity and carbon deposition. Increasing N_{Na+} beyond the optimum value leads to a decrease in catalytic activity, most likely due to the formation of stable surface carbonate species. This indicates that the beneficial effect of alkali-metal incorporation has a limit and is associated mainly with an increased concentration of oxidizing species on the catalyst surface and enhanced carbon gasification. Carbon deposition is minimized at moderate N_{Na+} values, whereas both

lower and higher concentrations result in increased coke formation. The highest coke amount is observed at the lowest N_{Na+}, which can be attributed to the relatively high rate of carbon formation compared with CO_2 gasification. This interpretation is supported by the higher residual CO_2 content in the reaction products for the corresponding sample. Correlation analysis shows a positive relationship between N_{Na+} and $T_{80\%}$ (r=+0.689), while coke formation correlates almost perfectly with the concentration of strong acidic sites (r=+0.999), confirming the important role of acidity in determining catalytic performance. Overall, the Na-form provides higher CH_4 conversion and the optimal N_{Na+} level ensures the best balance between carbon formation and gasification rates.

In addition to the synthetic zeolite-based systems, special attention was also paid to the use of natural zeolites as supports for Ni catalysts in DRM, with the Ni–CL system based on natural clinoptilolite being selected as a representative example.

Considering its structural and compositional characteristics, natural clinoptilolite represents an economically and technologically attractive alternative to conventional catalyst supports. For example, natural clinoptilolite (HEU-type) contains alkali and alkaline-earth metals (Na + K: 3.73–4.1 wt.%; Ca + Mg: 4.32–4.72 wt.%), which is comparable to the promoter content in industrial CH_4 conversion catalysts (up to 7 wt.%). In addition, its specific surface area (7–25 m^2/g) and well-developed microporous structure facilitate the formation of a highly dispersed nickel active phase [58].

Fig. 4 shows the X-ray diffraction pattern of the Ni–CL sample, and Fig. 5 presents (a) the SEM micrograph and (b) the corresponding EDX spectrum with the elemental composition of the Ni–CL catalyst.

Table-3: Dependence of catalytic activity and carbon deposition from the number of Na^+ ions.

N_{Na+} ($\times10^{22}$)	Max. CH_4 conversion (%)	X_{CH4} at 700^{0}C (%)	Residual CO_2 at 800 °C (%)	S_{CO} at 800^{0}C, (%)	Carbon deposition (g g^{-1} catalyst)
0,9	**100**	**79.2**	**14.6**	**45.4**	**0.058**
1,2	**100**	**83.0**	**7.7**	**45.2**	**0.009**
2,1	**86,8**	**71.8**	**8.9**	**42.5**	**0.011**

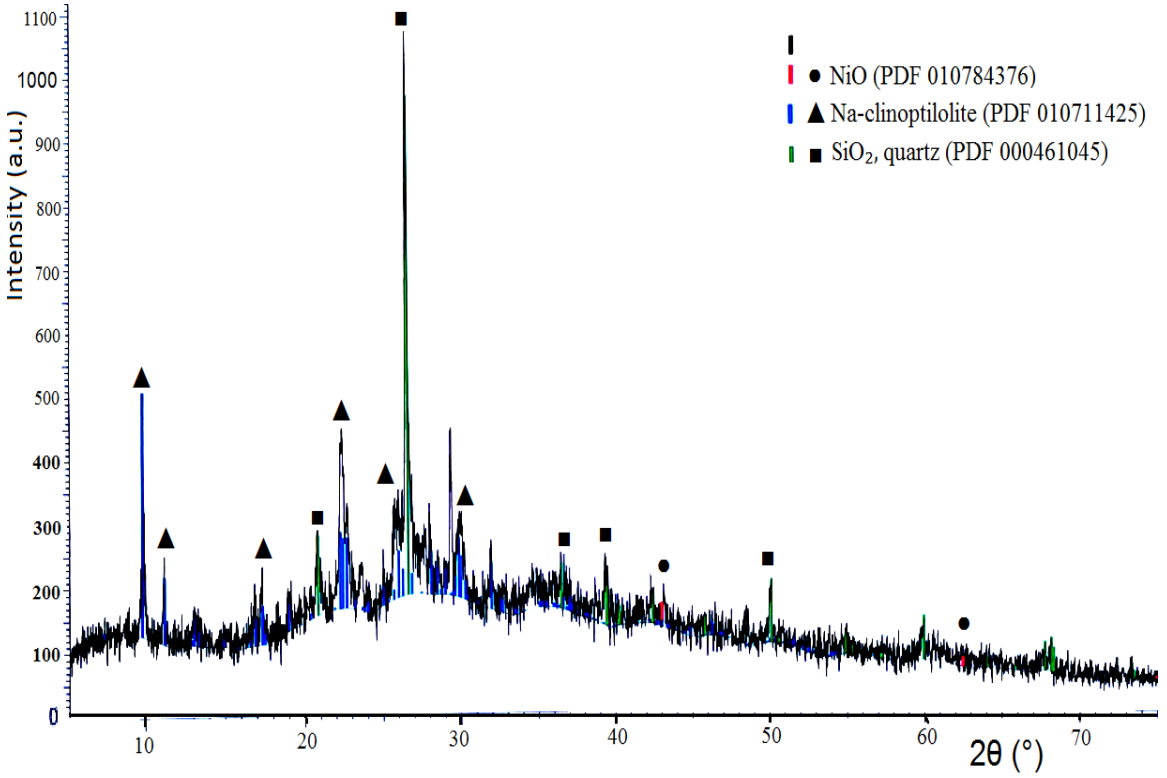

Fig. 4: X-ray diffraction patterns of Ni–CL sample.

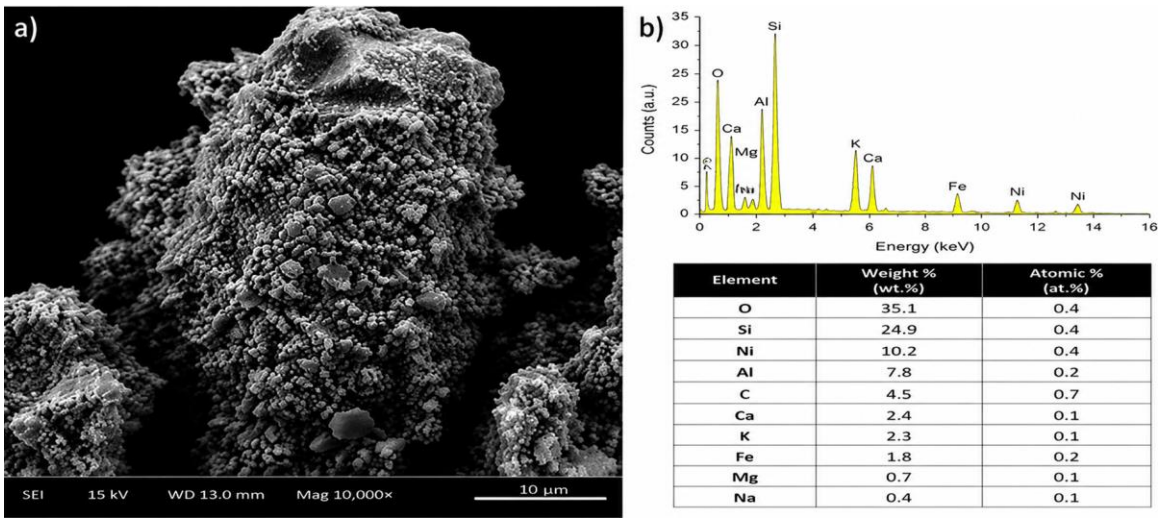

Element	Weight % (wt.%)	Atomic % (at.%)
O	35.1	0.4
Si	24.9	0.4
Ni	10.2	0.4
Al	7.8	0.2
C	4.5	0.7
Ca	2.4	0.1
K	2.3	0.1
Fe	1.8	0.2
Mg	0.7	0.1
Na	0.4	0.1

Fig. 5: (a) SEM micrograph and (b) corresponding EDX spectrum with elemental composition of Ni–CL sample.

The X-ray diffraction pattern of the Ni–CL sample (Fig. 4) confirmed preservation of the clinoptilolite framework after Ni introduction, indicating that the structure remains stable. Reflections of NiO were observed in the crystalline matrix, proving successful loading of the active phase; their low intensity suggests high dispersion or small Ni crystallite sizes.

SEM micrographs (Fig. 5 (a)) revealed agglomerated particles with a developed surface morphology and interparticle porosity. The EDX spectrum (Fig. 5(b)) showed the presence of Ni together with the main clinoptilolite framework elements (Si, Al, and O), exchangeable cations characteristic of the natural zeolite matrix, as well as minor components associated with micro-inclusions and mineral impurities. The percentages of elements in the sample were presented in the table. Overall, taken together with the XRD results, these observations indicate preservation of the HEU framework after Ni incorporation and the presence of the NiO phase in the composite.

Catalytic tests showed that complete CH_4 conversion over Ni–CL was achieved at 700 °C, while the temperature required to reach 80% conversion ($T_{80\%}$) is 615 °C (Fig.6). These values are consistent with the free volume fraction of the dehydrated zeolite (0.34) and suggest that the structural parameters of the zeolite matrix play an important role in determining catalytic performance. In comparison with Ni–MOR ($T_{80\%}$ = 695 °C; free volume fraction 0.28), clinoptilolite exhibits a more favorable combination of textural and acid–base properties.

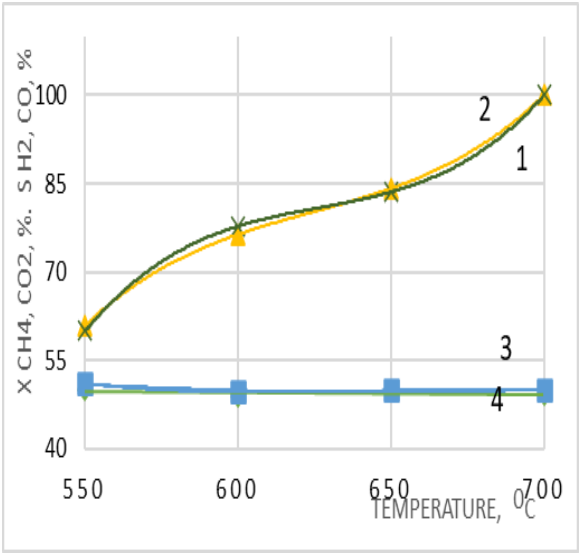

Fig. 6: Temperature dependence of CH_4 and CO_2 conversion and H_2 and CO selectivity over the Ni–CL catalyst in DRM. Curves: (1) CH_4 conversion, (2) CO_2 conversion, (3) CO selectivity, and (4) H_2 selectivity.

In addition, a separate systematic analysis was performed for clinoptilolite-based catalysts, where the influence of acid modification, SiO_2/Al_2O_3 ratio, pore characteristics, and total acidity on catalytic performance was investigated within the same structural framework.

Table-4: Effect of activating acid concentration on the physicochemical parameters of zeolite (CL) and characteristics of the resulting Ni-containing systems derived from them.

Sample	HCl concentration, M	SiO_2/Al_2O_3 ratio, mol/mol	Water adsorption capacity, mmol·g^{-1}	Limiting sorption volume, cm^3·g^{-1}	Ni–CL characteristics		
					*Total acidity ΣK_{NH_3}, mmol·g^{-1}	**$T_{80\%}$ for CH_4 conversion, ^{0}C	**CH_4 conversion (%) at 700 ^{0}C
CL	0	8.6	6.81	0.124	0.08	610	100
CL-0.5	0.5	10.1	6.65	0.121	-	680	84
CL-1	1	10.4	8.61	0.153	0.34	665	93
CL-2	2	11.7	8.90	0.161	0.12	540	100
CL-10	10	42.3	7.15	0.125	0.10	650	99

*Note: *The total acidity was evaluated based on NH_3 desorption measurements.*

***Catalytic performance parameters were obtained from DRM catalytic tests.*

The Ni–CL catalyst also exhibits stable CO_2 conversion and relatively high H_2 and CO selectivity over the investigated temperature range. This behavior indicates the effective participation of both reactants in the DRM process and confirms a favorable balance between methane activation and CO_2 conversion on the catalyst surface. The observed catalytic performance may be associated with the developed microporous structure of clinoptilolite, which facilitates dispersion of the active nickel phase. In addition, naturally occurring alkali and alkaline-earth components may promote CO_2 adsorption and its conversion during the DRM.

Chemical modification of the support with HCl solutions of different concentrations allowed the relationship between porous structure, SiO_2/Al_2O_3 ratio, surface acidity, and the catalytic activity of Ni–CL to be established. The results describing the changes in the porous structure of the support during acid activation, as well as their influence on the properties of Ni–CL, are summarized in Table 4.

It was shown that the sample with the optimal sorption space volume (sample CL-2) exhibited the lowest $T_{80\%}$ value together with complete CH_4 conversion at 700 °C, whereas excessive acid treatment (sample CL-10) leads to partial framework destruction and an increase in the SiO_2/Al_2O_3 ratio, accompanied by a decrease in both acidity and catalytic activity. A strong correlation was found between the total acidity of the support and the performance of the catalytic system ($r = -0.96$), as well as moderate correlations with the sorption volume ($r = 0.50$) and the SiO_2/Al_2O_3 ratio ($r = 0.47$). These results suggest that both structural and acid–base parameters contribute to the observed catalytic behavior of Ni–CL systems.

Special attention was paid to resistance toward carbon deposition. The amount of carbon deposits formed on samples CL-0 and CL-2, normalized per hour of catalyst operation, was estimated as 0.0066 and 0.008 $g \cdot g^{-1}cat \cdot h^{-1}$, respectively. These deposits were characterized by combustion temperatures of approximately 700 ± 50 °C, indicating their predominantly amorphous nature and relatively weak carbon–surface interactions, which may reduce the tendency toward rapid catalyst deactivation. Furthermore, the relationship between acidity and the amount of carbon deposited confirms the influence of acid sites on catalytic properties.

Thus, the Ni–CL systems combine several important advantages: high catalytic activity, resistance to coking, the absence of any need for additional promotion, and reduced material and energy demands of the process.

Overall, the comparative analysis of the investigated Ni/zeolite systems demonstrates that DRM performance depends on zeolite topology, acid–base properties, and the nature of exchangeable cations. While synthetic zeolites provide more uniform and controllable structural characteristics, natural clinoptilolite appears to be a promising support owing to its high catalytic activity, low coking tendency, and potential economic and environmental advantages.

Conclusion

In this study, the comparative structure–function relationships of Ni/zeolite composites in DRM were systematically investigated. Most studies of this kind focus on zeolites with a single framework type, whereas the present work provides a comparative analysis of the catalytic behavior of zeolites with different framework topologies and samples of one structural type with varying degrees of physicochemical modification.

A detailed analysis of Ni catalysts based on A-, X-, and Y-type zeolites showed that catalytic performance is governed primarily by zeolite structural features, including framework topology, pore architecture, and the nature of exchangeable cations, as well as by the concentration of basic and electron-acceptor surface sites. Quantitative correlations between framework type and both

methane conversion (r = 0.765) and residual CO_2 concentration (r = 0.815), as well as between the concentrations of basic and electron-acceptor sites and the H_2 yield (r = 0.93 and 0.91, respectively), confirm the key role of structural and surface properties in determining catalytic behavior.

Moreover, the favorable combination of framework topology, pore dimensions, and surface active sites in the Ni–CL, Ni–ZSM-5, and Ni–CaA systems affords particularly advantageous conditions for DRM.

For clinoptilolite-based systems, acid treatment enables controlled adjustment of the degree of dealumination and sorption volume, thereby favorable the balance between porosity and acidity and tuning the structure–property relationships of the resulting nickel composites.

These results further demonstrate the important role of zeolite framework characteristics and surface properties in determining the performance of Ni-based DRM catalysts.
From a practical perspective, the use of natural clinoptilolite may reduce both the cost and complexity of catalyst preparation, making it a promising inorganic support for nickel catalysts in DRM.

References:

1. A. Bhaskaran, S. A. Singh, B.M. Reddy and S. Roy, Integrated CO_2 Capture and Dry Reforming of CH_4 to Syngas: A Review, *Langmuir,* **40** (29), 14766–14778 (2024).
2. S.Yin, Challenges and future directions for green hydrogen development, *Academia Green Energy*, **2,** acadenergy7564 (2025).
3. Y. Gao, J. Jiang, Y. Meng, F. Yan, A. Aihemaiti, A review of recent developments in hydrogen production via biogas dry reforming, *Energy Conversion and Management,* **171,** 133-155 (2018).
4. R. Singh, A.Kumar and P. Patel, Biogas dry reforming for syngas production: Process perspectives and catalyst development. *Energy Conversion and Management*, **225,** 113438 (2020).
5. J. S. Brar, K.Singh, J. Wang and S. Kumar. Cogasification of Coal and Biomass: A Review, International *Journal of Forestry Research*, 363058 (2012) .
6. J-M. Lavoie, Review on dry reforming of methane, a potentially more environmentally-friendly approach to the increasing natural gas exploitation, *Frontiers in Chemistry,* **2** (81), 00081 (2014).
7. B. Agun and A. Abanades, Comprehensive review on dry reforming of methane: Challenges and potential for greenhouse gas mitigation, *International Journal of Hydrogen Energy,* **103,** 160 (2025).
8. X. Zhu, S. Liu and L.Wang, Recent advances in dry reforming of methane for syngas production. *Renewable and Sustainable Energy Reviews,* **134,** 110138 (2021).
9. H. Li, Q. Chen and Y. Huang, Dry reforming of methane: A review on process intensification and CO_2 utilization, *International Journal of Hydrogen Energy,* **47,** 28430–28458 (2022).
10. H. Seo, Recent Scientific Progress on Developing Supported Ni Catalysts for Dry (CO_2) Reforming of Methane. *Catalysts,* **8** (3), 110, (2018).
11. A. Khan, J. Shah and I. Ali, Nickel-based catalysts for dry reforming of methane: Recent advances and perspectives. *Applied Catalysis B: Environmental,* **308,** 121186 (2022).
12. S. Al-Fatish, A. A.Ibrahim, A. H. Fakeeha et al., Coke formation during CO_2 reforming of CH_4 over alumina-supported nickel catalysts, *Appl. Catal. A*, **364,** 150-155 (2009).
13. N. Boonsrisod, M. Phongaksorn, S. Tungkamani and T. Ratana Carbon Deposition over Ni/ZrO_2 Catalyst for Dry Reforming of Methane Reaction, *Burapha Science Journal*, **29** (1)**,** 310-326, (2024).
14. J. Niu, Z. Pan and K. Zhang Nanoconfined water in carbon capture and storage. *Academia Nano: Science, Materials, Technology*, **3,** AcadNano8073 (2026).
15. X. Fang, F. Qin, L. Peng, M. Lv and H. Zeng, Synergistic Promotion Strategies for Ni-Based Catalysts in Methane Dry Reforming: Suppressing Sintering and Carbon Deposition. *Processes,* **13,** 3322 (2025).
16. Z. Zhou, K. Li, H. Liu, Y. Jin, J. Wang, C. You and J. Niu, The evolution mechanism of carbon morphology and carbon deposition amount on nickel-based catalyst in dry reforming reaction, *International Journal of Hydrogen Energy,* **189,** 152142 (2025)
17. Y. Liu, H. Jin, L. Huang, Y. Liu, S. Cui, H. Liu, S. Zeng and L. Wang, Anti-coking Ni-La_2O_3/SiO_2 catalyst prepared by using a glycine-assisted impregnation method for low-temperature dry reforming of methane, *Chemistry Letters*, **53** (4), upae055 (2024).
18. H. Xiao, J. Dong, Y. Zhang, X. Cao, Y. Li, D. He, Y. Luo, P. Wang and H. Wang, Highly efficient Ni/Ac–Al_2O_3 catalysts in the dry reforming of methane: influence of acetic acid treatment and Ni loading. *RSC Adv.,* **14,** 39061 (2024).
19. C. Chen, W. Wang, Q. Ren, R. Ye, N. Nie, Z. Liu and J. Xiao, Impact of preparation method on

nickel speciation and methane dry reforming performance of Ni/SiO_2 catalysts. *Frontiers in Chemistry*, **10,** 993691 (2022).
20. H. Arbag, S. Yasyerli, N. Yasyerli, G. Dogu and T. Dogu, Enhancement of catalytic performance of Ni based mesoporous alumina by Co incorporation in conversion of biogas to synthesis gas, *Applied Catalysis B: Environmental*, **198,** 254-265 (2016).
21. M. Li, Z. Sun and Y. H. Hu, Catalysts for CO_2 reforming of CH_4: a review, *Journal of Materials Chemistry A*, **9** (21), D1TA00440A (2021).
22. D. Pakhare and J. Spivey, A review of dry (CO_2) reforming of methane over noble metal catalysts, *Chemical Society Reviews*, **43**, 7813–7837 (2014).
23. V. I. Yagodkin, Yu. G. Fedyukin, S. M. Sokolov, L. N. Shmakova and N. G. Anikin, Development of a New Generation of Catalysts for Tubular Furnaces of Hydrogen Plants, *Catalysis in Industry*, **5,** 28-31 (2004).
24. L. Zhang, Y. Zhou, H. Cui, Z. Cheng and Z. Zhou, Performance enhancement of $Ni/CaO-Al_2O_3$ dual-function materials for integrated CO_2 capture and conversion via dry reforming of methane, *Chemical Engineering Science*, **320,** 122635 (2026).
25. S. A. Solov'ev, R. N. Zatelepa, E. V. Gubaren, *et al*., Activity and stability of Ni/Al_2O_3 catalysts in carbon dioxide conversion of methane as influenced by alkali metal oxide additives (K_2O, Na_2O, Li_2O). *Russ J Appl Chem*, **80,** 1883–1887 (2007).
26. Z. Alipour, M. Rezaei and F. Meshkani, Effect of alkaline earth promoters (MgO, CaO, and BaO) on the activity and coke formation of Ni catalysts supported on nanocrystalline Al_2O_3 in dry reforming of methane, *Journal of Industrial and Engineering Chemistry*, **20** (5), 2858-2863 (2014).
27. Z. Hou, O. Yokota, T. Tanaka *et al*., Characterization of Ca-promoted $Ni/\alpha-Al_2O_3$ catalyst for CH_4 reforming with CO_2, *Appl. Catal. A.*, **2,** 381-387 (2003).
28. J. Juan-Juan, M. C. Roman-Martinez and M. J. Illan-Gomez, Effect of potassium content in the activity of K-promoted Ni/Al_2O_3 catalysts for the dry reforming of methane, *Appl. Catal. A*, **301** (1), 9-15 (2006).
29. Z. Hou, X. Zheng and T. Yashima, High coke-resistance of K-Ca-promoted $Ni/\alpha-Al_2O_3$ catalyst for CH_4 reforming with CO_2, *React. Kinet.and Catal. Lett.*, **84** (2), 229-235 (2005).
30. Y. A. Al-Baqmaa, A. S. Al-Fatesh, A. A. Ibrahim *et al*., Effects of MgO on Ni/Al_2O_3 catalysts for CO_2 reforming of methane to syngas. *Res Chem Intermed*, **49,** 5015–5028 (2023).
31. L. Zhou, L. Li, N. Wei, J. Li and J.-M. Basset, Effect of $NiAl_2O_4$ formation on Ni/Al_2O_3 stability during dry reforming of methane. *ChemCatChem*, **7**(16), 2508–2516 (2015).
32. P. Cao, H. Zhao, S. Adegbite, B. Yang, E. Lester and T. Wu, Stabilized CO_2 reforming of CH_4 on modified Ni/Al_2O_3 catalysts via in-situ K_2CO_3-enabled dynamic coke elimination reaction. *Fuel*, **298,** 120599 (2021).
33. Z. Alipour, F. Meshkani and M. Rezaei, Effect of K_2O on the catalytic performance of Ni catalysts supported on nanocrystalline Al_2O_3 in CO_2 reforming of methane. *Hydrogen, Fuel Cell & Energy Storage*, **2** (4), 264 (2016).
34. P. Frontera, A. Macario, A. Aloise, P. L. Antonucci, G. Giordano and J. B. Nagy, Effect of support surface on methane dry-reforming catalyst preparation, *Catalysis Today*, **218-219,** 18-29 (2013).
35. Y. Shen, S. Sun, F. Lian, Y. Liu and H. Qiu, Engineering Robust Ni–CaO Interaction Using Potassium for Low-Carbon Deposition Integrated CO_2 Capture and Dry Reforming of the Methane Process, *Industrial & Engineering Chemistry Research*, **65** (4), 2156-2168 (2026).
36. S. Khajeh Talkhoncheh, M. Haghighi, N. Jodeiri and S. Aghamohammadi, Hydrogen production over ternary supported Ni/Al_2O_3–clinoptilolite-CeO_2 nanocatalyst via CH_4/CO_2 reforming: Influence of support composition, *Journal of Natural Gas Science and Engineering*, **46,** 699-709, (2017).
37. D. Yao, H. Yang, H. Chen *et al*., Investigation of nickel-impregnated zeolite catalysts for hydrogen/syngas production from the catalytic reforming of waste polyethylene. *Applied Catalysis B: Environmental*, **227,** 477-487 (2018).
38. R. Alotaibi, F. Alenazey, F. Alotaibi, N. Wei, A. Al Fatesh and A. Fakeeha, Ni catalysts with different promoters supported on zeolite for dry reforming of methane. *Applied Petrochemical Research*, **5** (4), 329–337 (2015).
39. G. Moradi, F. Khezeli and H. Hemmati, Syngas production with dry reforming of methane over Ni/ZSM-5 catalysts. *Journal of Natural Gas Science and Engineering*, **33,** 657–665 (2016).
40. S. Kweon, H. An, C. H. Shin *et al*., Nitrided Ni/N-zeolites as efficient catalysts for the dry reforming of methane. *Journal of CO_2 Utilization,* **51,** 101478 (2021).
41. P. Pizarro, M. Romay, D. P. Serrano and J. M. Escola, Dry reforming of methane over Ni/MFI catalysts: Role of the zeolite support acidity. *Catalysis Today*, **460,** 115481 (2025).
42. A. C. P. Guimarães, L. R. F. Coelho, A. A. A. Silva, Y. Xing, R. C. Colman, C. A. Henriques and L. V. Mattos, Dry reforming of methane over Ni catalysts supported on hierarchical ZSM-5 and

USY zeolites. *Catalysis Today*, **447,** 115159 (2025).

43. Kh. M. Minachev and Ya.I. Isakov, *Metal-containing zeolites in catalysis*, Nauka Press, Moscow, p. 112 (1975).
44. Q. Cheng, X. Yao, L. Ou, Z. Hu, L. Zheng, G. Li, N. Morlanes, J. L. Cerrillo, P. Castaño, X. Li, J. Gascon and Y. Han, Highly Efficient and Stable Methane Dry Reforming Enabled by a Single-Site Cationic Ni Catalyst, *J Am Chem Soc.*, **145** (46), 25109-25119 (2023).
45. J. Zhang, Y. Li, H. Song, L. Zhang, Y. Wu, Y. He, L. Ma, J. Hong, A. Tayal, N. Marinkovic, D. E. Jiang, Z. Li, Z. Wu and F. Polo-Garzon, Tuning metal-support interactions in nickel-zeolite catalysts leads to enhanced stability during dry reforming of methane, *Nat Commun.*, **15** (1), 8566 (2024).
46. G. Li, H. Hao, P. Jin, M. Wang, Y. Yu and C. Zhang, Dry reforming of methane over Ni/Al_2O_3 catalysts: Support morphological effect on the coke resistance. *Fuel*, **298**, 130855 (2024).
47. S. L. Hasan, M. N. Wijayanti, Y. Hendrawan, I. Handayani, E. Sanwani and N. Halim, Synthesis of coal fly ash derived NaX zeolite as a nickel catalyst support in CO_2 methanation, *Journal of Environmental Chemical Engineering*, **13** (6), 119654 (2025).
48. P. Zang, J. Tang, X. Xing, X. Wang, G. Qi, P. Zhao, L. Cui, S. Chen and Y. Dong, Design of Ni-FAU Zeolite Bifunctional Materials for Integrated Carbon Dioxide Capture and Methanation: Construction of ultrafine NiO nanoparticles, *Journal of Colloid and Interface Science*, **692,** 137509 (2025).
49. L. Wei, N. Kumar, W. Haije, J. Peltonen, M. Peurla, H. Grénman and W. de Jong, Effect of synthesis methods on the physicochemical and catalytic properties of Ni 13X and Ni 5A zeolite catalysts in CO_2 methanation, *Catalysis Today*, **452,** 115239 (2025).
50. S. N. Orlik, Combined effect of the redox and acid-base properties of catalysts in redox conversions of nitrogen oxides and methane, *Kinetics and Catalysis*, **49,** 537-544 (2008).
51. M. V. Vishnetskaya, A. N. Emelyanov, N. V. Shcherbakov, Yu. N. Rufov and A. N. IlIchev, The role played by singlet oxygen in transformations of hydrocarbons on zeolites, *Russian Journal of Physical Chemistry*, **78** (12), 1918-1923 (2004).
52. S. Wang, Y. He, W. Jiao and J. Wang, Recent experimental and theoretical studies on Al siting/acid site distribution in zeolite framework, *Current Opinion in Chemical Engineering*, **23,** 146-154 (2019).
53. C. Auepattana-Aumrung, V. Márquez, S. Wannakao, B. Jongsomjit, J. Panpranot and P. Praserthdam, Role of Al in Na-ZSM-5 zeolite structure on catalyst stability in butene cracking reaction. *Sci Rep.*, **10** (1), 13643 (2020).
54. W. Lai, L. Wang, Z. Dai, L. Yao, L. Yang and W. Jiang, The mitigation of carbon deposition for Ni-based catalyst in CO_2 reforming of methane: A combined experimental and DFT study, *Carbon Capture Science & Technology*, **13,** 100286, (2024).
55. X. Fang, F. Qin, L. Peng, M. Lv and H. Zeng, Synergistic Promotion Strategies for Ni-Based Catalysts in Methane Dry Reforming: Suppressing Sintering and Carbon Deposition. *Processes*, **13,** 3322 (2025).
56. Y. Liu, H. Jin, L. Huang, Y. Liu, S. Cui, H. Liu, S. Zeng and L. Wang, Anti-coking $Ni\text{-}La_2O_3/SiO_2$ catalyst prepared by using a glycine-assisted impregnation method for low-temperature dry reforming of methane, *Chemistry Letters*, **53** (4), upae055 (2024).
57. F. Guo, Y. Zhang and J. Li, Dry reforming of methane over Ni-based catalysts: Role of support and surface properties. *Chemical Engineering Journal*, **452,** 139304 (2023).
58. S. T. Rustamova, M. M. Akhmedov and N. I. Abbasova, Zeolite of chabazite-type synthesis and catalysts on zeolite basis properties investigation in the proses of conversion of methane by carbon dioxide, *Energy Technologies and Resource Saving*, **6,** 35-38 (2010).
59. S. Tokao and M. Mosaichi, Method for simplified and accelerated measurement of solid acids using differential thermobalance, *J. Bunseki kiki*, **5** (7), 59–64 (1969).
60. M. M. Akhmedov, S. T. Rustamova and I. A. Talybly, On the issue of improving the gas chromatographic scheme for separating a multicomponent mixture obtained during the conversion of methane into synthesis gas, *Journal of Chemical Problems*, **1,** 41-45 (2009).
61. J. G. Bendoraitis, A. W. Chester, F. G. Dwyer and W. E. Garwood, Size and Shape Effects in Zeolite Catalysis. *Studies in Surface Science and Catalysis*, **28**, 669-675 (1986).